A phosphorylated zinc finger peptide bearing a gadolinium complex for zinc detection by MRI.

Kyangwi Malikidogo, Agnès Pallier, Frédéric Szeremeta, Célia S Bonnet, Olivier Sénèque

A phosphorylated zinc finger peptide bearing a Gadolinium complex for Zinc detection by MRI

Kyangwi P. Malikidogo,[a] Agnès Pallier,[b] Frédéric Szeremeta,[b] Célia S. Bonnet*[b] and Olivier Sénèque*[a]

[a] Univ. Grenoble Alpes, CNRS, CEA, IRIG, LCBM (UMR 5249), F-38000 Grenoble, France.

[b] Centre de Biophysique Moléculaire, CNRS (UPR 4301), Université d'Orléans, F-45041 Orléans

Email: *olivier.seneque@cea.fr* and celia.bonnet@cnrs.fr

Abstract

Two zinc finger peptides, namely ZFQD^{Ln} and ZFQE^{Ln} (Ln = Tb or Gd) with an appended Ln^{3+} chelate and a phosphoserine able to coordinate the Ln^{3+} ion are presented. The two peptides differ by the amino acid anchorage of the chelate, either aspartate (D) or Glutamate (E). Both peptides are able to bind Zn^{2+} and adopt the □□□ fold. Interestingly, ZFQE^{Tb} shows a decrease in sensitized Tb^{3+} luminescence upon Zn^{2+} binding whereas ZFQD^{Tb} does not. The luminescence change upon Zn^{2+} binding is attributed to a change of hydration number (q) of the Tb^{3+} ion due to the decoordination of the phosphoserine from the Ln^{3+} ion upon Zn^{2+} binding and peptide folding. This process is highly sensitive to the length of the linker between the Ln chelate and the peptidic backbone. The magnetic properties of the gadolinium analogue ZFQE^{Gd} were studied. An impressive relaxivity increase of 140 % is observed at 60 MHz and 25°C upon Zn^{2+} binding. These changes can be attributed to a combined increase effect of the hydration number of Gd^{3+} and of the rigidity of the system upon Zn^{2+} binding. Phantom MR images at 9.4 T show a clear signal enhancement in the presence of Zn^{2+}. These zinc finger peptides offer a unique platform to design such Zn-responsive probes.

Introduction

Zinc is the second most abundant transition metal ion in human body after iron.[1,2] It is mostly bound to proteins that play a central role in controlling gene transcription and metalloenzyme function. Zn^{2+} is a signaling ion involved in several pathways such as the immune system,[3] glutamatergic neurons, fertilization[4] and early development processes.[5,6] Zn^{2+} concentration is highly regulated and disruptions in its homeostasis have been implicated in several diseases such as pancreatic, prostatic and breast cancers,[7] diabetes[5] or neurodegenerative diseases, to cite a few. Therefore the non-invasive visualization of Zn^{2+} *in vivo* is of prime importance for the early detection of these diseases[8] and more generally to better understand the role of zinc in biomedical research.

Magnetic resonance imaging is a powerful technique due to its high resolution, which plays a central role in molecular imaging. The last years have witnessed tremendous developments of MRI contrast agents sensitive to Zn^{2+}, pushed forward by its successful *in vivo* detection.[9] Paramagnetic Gd^{3+} chelates are by far the most exploited contrast agents for Zn^{2+} detection. In most of the examples, Gd^{3+} is complexed by a macrocyclic derivative of DO3A (1,4,7,10 tetraazacyclododecan-1,4,7,10 tricarboxylic acid), to which a Zn^{2+} sensitive moiety such as dipicolylamine, iminodiacetate or quinoline is linked.[10] The efficacy, called relaxivity, of such agents is mainly influenced by the number of water molecules directly coordinated to Gd^{3+}, its water exchange rate with the bulk, and the rotational correlation time of the complex influenced by the size and rigidity of the system. Upon Zn^{2+} binding, at least one of these microscopic parameters must be modified to give a responsive contrast agent. The most successful contrast agent used *in vivo* relies on a change of the rotational correlation time due to the formation, in the presence of Zn^{2+}, of a ternary complex with Human Serum Albumin (HSA), which is the most abundant protein in the blood. Such response is maximum at medium magnetic field (20-80 MHz), where the effect of the rotation is the most important. As relaxivity is directly proportional to *q*, the number of water molecule coordinated to Gd^{3+}, the modification of this parameter gives rise to dramatic changes upon Zn^{2+} binding that are similar over the whole field range. Such strategy has been explored successfully to achieve high relaxivity increase at 7T,[11] where the resolution is better. However, the prediction of the modification of *q* in the presence of Zn^{2+} remains very difficult and many synthetic efforts should be done to obtain one successful complex.

We have recently developed, in a completely different approach, a Zn^{2+} sensor for dual MRI and luminescence detection based on a zinc finger scaffold ($LZF2^{Ln}$, Ln = Tb or Gd, see Fig. S1 of SI for its sequence).[12] The folding of the peptide upon Zn^{2+} binding results in a modification of the rotational correlation time of the system that is detectable by MRI. Inspired by the work of Vázquez et al.[13] for the detection of phosphorylation using a luminescent Tb^{3+} complex, we anticipated that using this versatile zinc-finger scaffold, we could develop a system based on a change in the hydration number *q*, taking advantage of the replacement of a Gd-bound water molecule by the phosphate group of a phosphoserine, similarly to Vazquez's probe.

We have therefore synthesized two candidate contrast agents, $ZFQD^{Gd}$ and $ZFQE^{Gd}$. They are 27-amino acid classical ββα zinc finger (ZF) peptides comprising a phosphoserine and functionalized by a Gd^{3+} DO3A-propylamine chelate. These two contrast agents differ only by the amino acid to which the Gd^{3+} chelate is attached, which is either an aspartate (D) or a glutamate (E) (Fig. 1A). Classical ββα zinc fingers have no defined conformation in their Zn^{2+}-free form while they adopt a compact ββα fold upon Zn^{2+} binding to two histidines and two cysteines.[14–16] The DO3A propylamine ligand leaves available a coordination site for phosphoserine binding to the lanthanide ion, and we anticipated that the conformational changes upon Zn^{2+} binding would modify the Gd^{3+}-phosphoserine distance resulting in a change in the Gd^{3+} coordination.

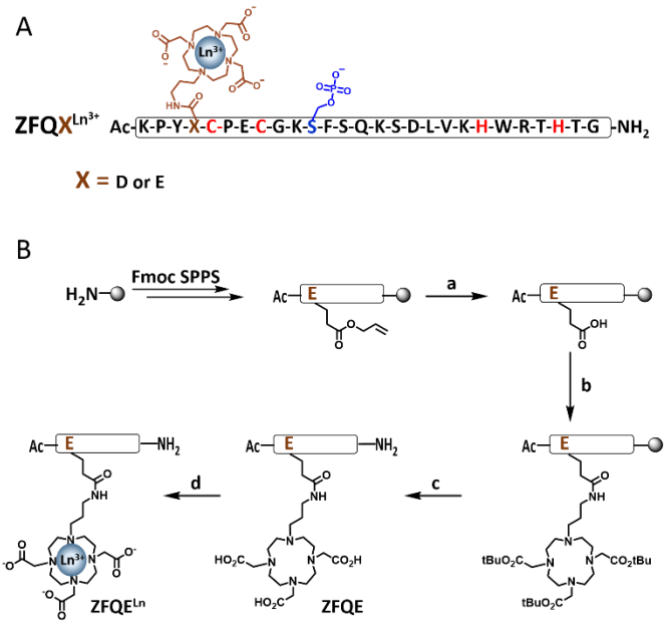

Fig. 1: (A) Amino acid sequence of ZFQX^{Ln} (X = D or E, Ln^{3+} = Tb^{3+} or Gd^{3+}). Zn^{2+}-binding cysteines and histidines are shown in red. The amino acid bearing the Ln(DO3A-propylamide) complex is shown in brown. Phosphate group in blue was incorporated in the peptide sequence to induce a variation of *q*. (B) Synthetic pathway for the preparation of ZFQE^{Ln} (or ZFQD^{Ln}) using Fmoc SPPS strategy. Conditions: a) $Pd(PPh_3)_4$, phenylsilane, degassed anhydrous DCM, 2x 1h, at room temperature; b) DO3A(tBu)$_3$-propylamine[13,17], PyBOP, DIEA, DMF, overnight at room temperature; c) TFA/H_2O/triisopropylsilane/thioanisole/dithiotreitol, 4h at room temperature; d) $LnCl_3.xH_2O$, H_2O, pH 6.2, overnight. ZFQD was obtained following the same procedure but using Fmoc-Asp(OAllyl)-OH instead of Fmoc-Glu(OAllyl)-OH.

Results and discussion

Synthesis of Ln-ZF complexes: The sequence of ZFQD or ZFQE is based on the consensus sequence of Zinc Fingers described by Berg et al.[14] The synthesis of ZFQE is described in Fig. 1B. The peptide was elongated on Rink Amide resin following standard Fmoc/*t*Bu solid-phase synthesis procedures (SPPS).[18] A glutamate amino acid with its side chain protected as an allyl ester, orthogonal to other protecting groups, was insert after the N-terminal cysteine. The peptide was acetylated after the N-terminal lysine. The removal of Alloc group was performed using Pd^0.[19] The *t*Bu-protected DO3A-propylamine pro-ligand, which was synthesized according to literature procedures,[13,17] was then coupled to the free carboxylic acid of the peptide using PyBOP/DIEA activation. Finally, the peptide was deprotected and cleaved from the resin in a mixture of trifluoroacetic acid (TFA) and scavengers, purified by reverse phase high performance liquid chromatography (HPLC) and characterized by ESI-MS (Fig. S2 of SI). Ln^{3+} complexes were obtained by reaction of ZFQE with $LnCl_3$, xH_2O in water pH 6.2 overnight. ZFQD^{Tb} was synthesized the same way only, an Asp residue was used instead of a Glu.

Zn^{2+} binding properties: First, the Zn^{2+} binding properties of the ZFQE^{Tb} and ZFQD^{Tb} were investigated by circular dichroism (CD) and luminescence spectroscopy. CD spectra in the absence and in the presence of 1.5 equivalent of Zn^{2+} were recorded in water containing 250 µM *tris*(2-carboxyethyl)phosphine (TCEP) at pH 7.4 (Fig. 2A and 2C). The CD spectra of both Zn^{2+}-free peptides are characteristic of an unstructured (random coil)

classical ββα zinc finger peptide with an intense negative CD signal at 200 nm and a small shoulder starting at *ca.* 225 nm.[20] Addition of excess of Zn^{2+} induces a change in the CD spectra with a minimum at 205 nm and a shoulder at 220 nm, which is characteristic of Zn-bound ββα zinc fingers.[20] This indicates that the presence of both Tb^{3+}(DO3A-propylamide) complex and phosphoserine does not alter the behaviour and folding ability of the zinc finger peptide. Zn^{2+} binding to $ZFQE^{Tb}$ and $ZFQD^{Tb}$ was investigated in HEPES buffer (10 mM, pH 7.4) containing TCEP (250 µM) by tryptophan fluorescence and Tb^{3+} luminescence under 280 nm excitation (Fig. 2B and D; Fig. S3 and S4 of SI). For $ZFQE^{Tb}$, tryptophan fluorescence displays almost no change upon Zn^{2+} addition (Fig. S3 of SI). Contrastingly, the sensitized Tb^{3+} luminescence of $ZFQE^{Tb}$ decreases linearly upon addition of Zn^{2+} up to approximatively 0.9 equivalent and then remains constant upon further addition of Zn^{2+}, thus monitoring formation of the expected 1:1 Zn/peptide complex (Fig. 2B). A 55% quenching of Tb^{3+} emission is observed upon Zn^{2+} binding to the peptide. For $ZFQD^{Tb}$, neither tryptophan fluorescence nor Tb^{3+} emission showed variation in their intensity upon Zn^{2+} binding, despite Zn^{2+} binding observed by CD.

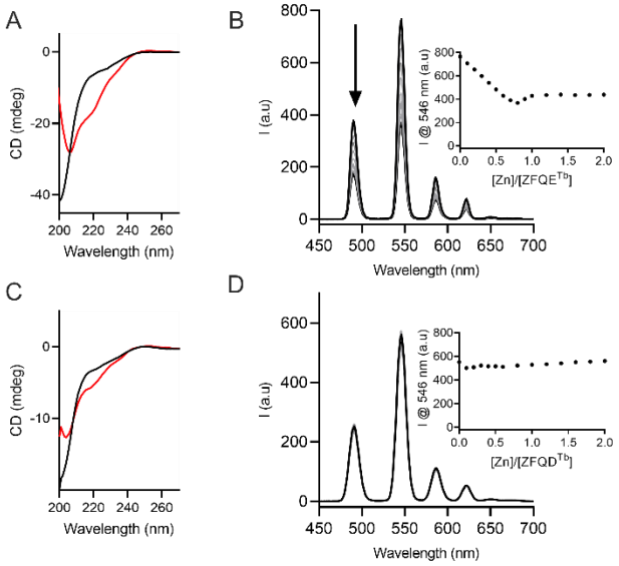

Fig. 2: (A) CD spectroscopic characterization of $ZFQE^{Tb}$ (20 µM) without Zn^{2+} (black) and in the presence of 1.5 eq. of Zn^{2+} (red). (B) Evolution of time-resolved Tb^{3+} luminescence emission spectra (λ_{ex}= 280 nm, delay = 100 µs) upon addition of Zn^{2+} in a solution of $ZFQE^{Tb}$ (20 µM). (C) CD spectroscopy characterization of $ZFQD^{Tb}$ (10 µM) without Zn^{2+} (black) and in the presence of 1.5 eq. of Zn^{2+} (red). (D) Evolution of time-resolved Tb^{3+} luminescence emission spectra (λex = 280 nm) upon addition of Zn^{2+} solution in $ZFQD^{Tb}$. Solutions were prepared in unbuffered water pH 7.4 for CD and HEPES buffer (10 mM, pH 7.4) for luminescence. All samples contained TCEP (250 µM).

In order to understand these results, the hydration number, *q*, was determined for the Zn-free and Zn-bound forms of $ZFQE^{Tb}$ and $ZFQD^{Tb}$ by difference in Tb^{3+} luminescence lifetimes in H_2O and D_2O (Table 1 and Fig. S5 of SI). Regarding $ZFQD^{Tb}$, both the Zn-free and Zn-bound forms displayed mono-hydrated Gd chelates ($q \approx 1.0$), consistent with the absence of variation in the luminescence emission of this probe. However, *q* values of 0.4 ± 0.2 and 1.0 ± 0.2 were obtained for $ZFQE^{Tb}$ and Zn-$ZFQE^{Tb}$, respectively. The increase of *q* upon Zn^{2+} binding to $ZFQE^{Tb}$, is consistent with the decrease of the Tb^{3+} luminescence intensity observed, indicating a change in the coordination sphere of Tb^{3+} upon Zn^{2+} binding. It is known that phosphate groups bind Ln^{3+} and other cations in a monodentate fashion.[21,22] Therefore, we can propose that in the Zn-bound form, a water molecule is coordinated

to the Tb^{3+} ion in addition to the four cyclen nitrogen atoms and the four carbonyl oxygen atoms of the pendent arms, while in the Zn-free form, an equilibrium may take place between two species, one with the phosphoserine bound to Tb^{3+} and the other with a water molecule coordinated instead (Fig. 3). Contrastingly, for $ZFQD^{Tb}$, which has a shorter anchorage for the Tb^{3+} chelate (one less methyl), the phosphoserine does not coordinate Tb^{3+} in the presence or in the absence of Zn^{2+}. This indicates that the length of the anchorage is crucial to observe the coordination of the phosphoserine and a significant *q* change.

Table 1: Luminescence lifetimes and derived *q* values for free and Zn-loaded ZFQD and ZFQE probes in HEPES buffer (10 mM, pH 7.4) and 250 µM of TCEP. Error on lifetime is estimated ± 0.03 and error on *q* is estimated ± 0.2.

Compounds	τ_{Tb} in H_2O	τ_{Tb} in D_2O	*q*
$ZFQD^{Tb}$	1.14 ms	1.69 ms	1.1
Zn-$ZFQD^{Tb}$	1.09 ms	1.54 ms	1.0
$ZFQE^{Tb}$	1.79 ms	2.39 ms	0.4
Zn-$ZFQE^{Tb}$	1.47 ms	2.35 ms	1.0

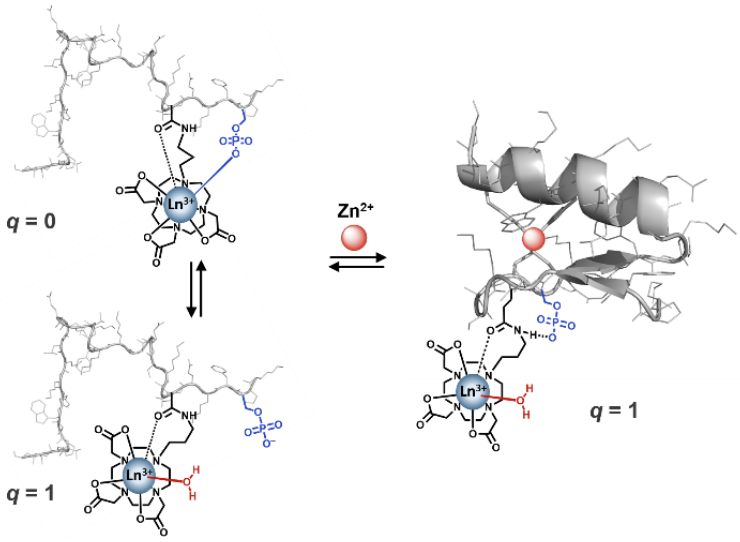

Fig. 3: Principle of Zn^{2+} detection: Folding of the $ZFQE^{Ln}$ probe and variation of *q* induced by Zn^{2+}-binding. In the Zn^{2+} free state, an equilibrium between q = 0 and q = 1 may take place.

Magnetic properties: In light of these encouraging results, we envisioned that replacing the Tb^{3+}-ion in $ZFQE^{Tb}$ by a Gd^{3+} ion, a Zn^{2+}-responsive MRI probe would be obtained. A Zn^{2+} titration of $ZFQE^{Gd}$ in HEPES buffer pH 7.4 monitored by ^1H relaxivity at 60 MHz and 25°C was performed (Fig. 4A). The relaxivity increases up to one equivalent of Zn^{2+} added and remains constant above this limit. This result is consistent with the luminescence titration of $ZFQE^{Tb}$ (Fig. 2B) presented above and confirms the formation of 1:1 $Zn^{2+}/ZFQE^{Gd}$ complex. The relaxivity of the system at 60 MHz and 25°C in the absence of Zn^{2+} is 10.48 mM^{-1} s^{-1}, and 25.27 mM^{-1} s^{-1} in the presence of 1 eq of Zn^{2+}, which represents an increase of more than 140%. As expected, this is better than the previous zinc-finger system that we developed and based solely on a change of the rotational correlation time of the system. But it ranges also among the best system found in the literature, especially based on a change of the number of water molecule coordinated.[10,23,24]

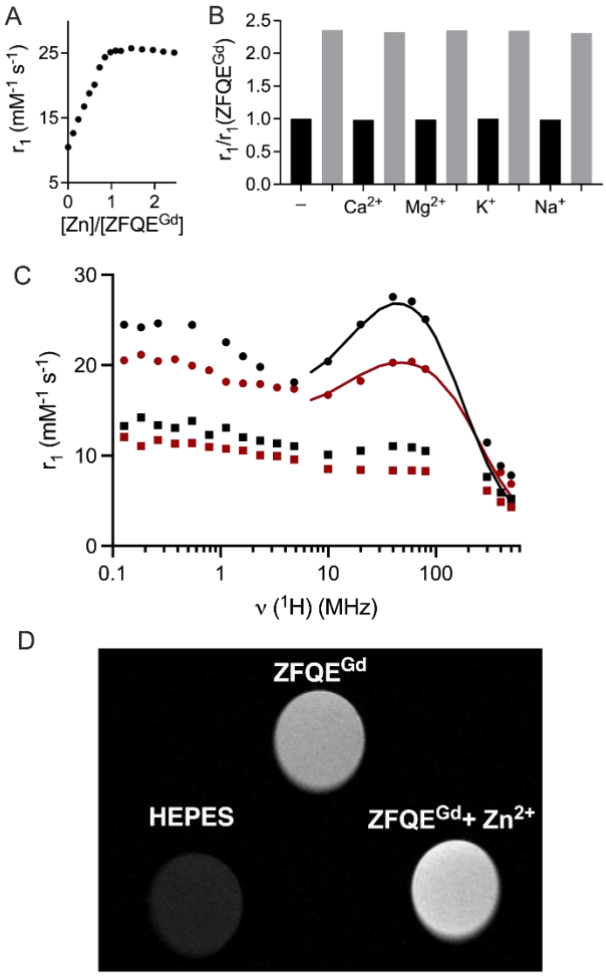

Fig. 4: (A) ^{1}H relaxivity measurements (60 MHz, 25°C) of a solution of ZFQE^{Gd} (0.69 mM) in HEPES buffer solution (100 mM, pH 7.4, 25 mM TCEP) with increasing amount of Zn^{2+}. (B) Selectivity plot obtained by measuring the relaxivity of ZFQE^{Gd} (0.38 mM) alone (left) or in the presence of various physiological cations (1 eq.) before (black) and after (grey) addition of Zn^{2+} (1 eq.). (C) ^{1}H NMRD profiles at 25°C (black symbols) and 37°C (red symbols) for Zn-free (square) and Zn-loaded (circle) ZFQE^{Gd} (0.69 mM). The solid lines represent the least squares fit of the data points using the SBM theory. Solutions were prepared in HEPES buffer (100 mM, pH 7.4) containing TCEP (25 mM). All solutions were prepared in HEPES buffer solution (100 mM, pH 7.4, 25 mM TCEP). D) T1-weighted MR images of phantoms containing ZFQE^{Gd} (240 µM) in the absence or in the presence of 1.5 eq of Zn^{2+}, in a HEPES buffer (100 mM, pH = 7.4) containing TCEP (30 mM). Images were acquired at 9.4 T using spin echo sequence with TE = 9.9 ms, TR = 50 ms.

In order to better understand the origin of this relaxivity response, the ^{1}H NMRD profiles of ZFQE^{Gd} were recorded at two temperatures and over a wide range of magnetic fields (0.1 to 500 MHz) (Fig. 4C). First, we can see that both in the absence and in the presence of Zn^{2+}, the system shows the typical hump of slowly rotating species. This was expected in the presence of zinc, as there is one water molecule coordinated to Gd^{3+}, and the system is certainly endowed with a high rotational correlation time due to the folding. In the absence of zinc, this confirms that there is certainly an exchange between 0 and 1 water molecule coordinated and/or participation of second sphere water molecules to the overall relaxivity. This is consistent with the luminescence results (q = 0.4). Conversely to what is normally obtained for systems based on a change in the hydration number, the relaxivity increase is not constant over the whole range of magnetic field. The maximum increase is obtained at medium field (40-60 MHz; ca. 150 %), while at high field (400 MHz), the relaxivity increase is 50 and 67 % at 25°C and

37°C, respectively. This shows that both the number of water molecules coordinated to Gd^{3+}, but also the rotational correlation time (τ_R), linked to the size and the rigidity of the complex plays a role in the response upon Zn^{2+} binding.

This is interesting as the coordination of the phosphoserine certainly plays a role in the preorganisation of the system in the absence of Zn^{2+}, but the folding in the presence of Zn^{2+} still gives rise to a sizeable response. The full fitting of the data in the absence of zinc is not reasonable to obtain a reliable picture of system due to the possible dynamic of exchange. In the presence of Zn^{2+}, it is impressive to note that the relaxivity of $ZFQE^{Gd}$ at 40 MHz 25°C is nearly twice that of $LZF2^{Gd}$ (27.56 vs 14.64 $mM^{-1}.s^{-1}$), and it is 30 % higher at 37°C (20.3 vs 15.75 $mM^{-1}.s^{-1}$).[12]

In the case of $LZF2^{Gd}$,[12] we had shown that the water exchange rate was limiting the relaxivity in the presence of Zn^{2+}, which is not the case here as the relaxivity decreases with increasing temperature even in the presence of Zn^{2+}. This was expected as the water exchange rate of this monohydrated DO3A-alkylamide system is two orders of magnitude faster than that of DO3A-monoamide.[25] Interestingly, the fitting of the data using the Solomon-Bloembergen and Morgan theory was possible without the incorporation of the Lipari-Szabo treatment, which underlines the very high rigidity of the system. The best fit parameters obtained from the analysis of the ^1H NMRD data are summarized Table 2 and Table S1. The fitted curves are presented Fig. 4C. The rotational correlation time obtained matches well with the global rotational correlation time obtained for $LZF2^{Gd}$. It shows that for $ZFQE^{Gd}$ in the presence of Zn^{2+}, there is no loss of relaxivity due to internal flexibility of the system. This could be rationalized by the formation of a hydrogen bond between the phosphoserine and the alkylamide that would lock the Gd^{3+} complex (Fig. 3). The very high relaxivities achieved here in the presence of Zn^{2+} are due to a combination of a very rigid system with a high rotational correlation time and a fast water exchange rate. Moreover, the Zn^{2+}-induced response is not influenced by the presence of physiological cations such as Ca^{2+}, Mg^{2+}, Na^+ or K^+ (Fig. 4B). The addition of biologically relevant concentration of Cu^{2+} (0.15 eq.) does not modify the response, while the addition of 1 eq results in a 20 % relaxivity decrease (Fig. S6 of SI). Finally, phantom images were performed in vitro at 9.4 T on a MRI scanner and are presented Fig. 4D. A clear signal intensity enhancement for Zn-$ZFQE^{Gd}$ vs $ZFQE^{Gd}$ can be seen, and the T1 measurements (Fig. S7) performed in these conditions unambiguously confirm these results.

Table 2: Best-fit parameters obtained from the fitting of the ^1H NMRD profiles to the SBM theory.

	Zn-$ZFQE^{Gd}$	Zn-$LZF2^{Gd}$
r_1 (40 MHz, 25°C)/ $mM^{-1}.s^{-1}$	27.56	14.69
E / $kJ.mol^{-1}$ [a]	22 ± 4	13
τ^{298} / ps [b]	990 ± 50	1160
E_l/ $kJ.mol^{-1}$	–	20
τ_l^{298} / ps	–	145

[a] The values correspond to E_r for Zn-$ZFQE^{Gd}$ and E_g for Zn-$LZF2^{Gd}$; [b] The values correspond to τ_r for Zn-$ZFQE^{Gd}$ and τ_g for Zn-$LZF2^{Gd}$

Conclusion

To conclude, we have designed a Zn-responsive contrast agent based on a zinc finger peptide. The high response achieved is based on a switch in the phosphoserine coordination to the Ln^{3+}, which gives rise to a *q* change, and is amongst the best reported to date. The *in vitro* phantom images clearly show a sizeable increase of MRI efficacy at high field in the presence of Zn^{2+}, due to a combined effect of an increase in the Gd^{3+} hydration

number and in the rigidity of the molecule. Efforts to optimise the probe response are underway. The versatility of the peptide scaffold is an undeniable asset to achieve such goal with minimal synthetic efforts as illustrated by the change of a single amino acid to alter the response. The zinc finger scaffold offers a unique opportunity to design and optimise various zinc-responsive probes.

Materials and methods

Reagents and solvent: All commercial reagents were used as received from suppliers unless otherwise indicated. NovaPEG Rink Amide resin, N-α-9-fluorenylmethoxycarbonyl (Fmoc)-protected amino acids for peptide synthesis and 2-(6-Chloro-1-H-benzotriazole-1-yl)-1,1,3,3-tetramethylaminium hexafluorophosphate (HCTU) coupling reagent were obtained from Novabiochem or Iris Biotech. Cyclen was purchased from CheMatech. Other chemicals and solvents were purchased from Sigma-Aldrich.

Analyses and purification: TLC sheets ALUGRAM SILG/ ultraviolet (UV_{254}) were used for thin layer chromatography and visualized using UV light. Purification of organic compounds was performed on classic silica gel chromatography. ^{1}H and ^{13}C NMR spectra were recorded in deuterated solvents on a Bruker UltraShield Plus 400 Spectrometer operating at 400 and 100 MHz for ^{1}H and ^{13}C, respectively. All experiments were performed at 25 °C. Analytical HPLC separations were performed on an Agilent 1260 Infinity II system using XBridge BEH C18 (2.5µm, 4.6 x 7.5 mm) columns at 1 mL/min equipped with MS module. Preparative HPLC separations were performed on a VWR LaPrepΣ system using a Waters XBridge Peptide BEH130 C18 (5 µm, 150 mm x 19 mm) column at 14 mL/min. Mobile phase consisted in a gradient of solvent A (0.1% trifluoroacetic acid (TFA) in H_2O) and B (0.1% TFA in acetonitrile (MeCN)/H_2O 9:1). For analytical separations, Method A consisted in 5% B during 2 min followed by a 5 to 100 % B gradient in 13 min. Eluate was monitored by electronic absorption at 214, 254 and 280. LRMS (ESI) analyses were performed on a Thermo LXQ spectrometer. Circular dichroism (CD) spectra were recorded on an Applied Photophysics Chirascan spectropolarimeter equipped with a thermo-regulated cell holder. Emission and excitation spectra and Tb^{3+} luminescence lifetimes were measured on a Varian Cary Eclipse spectrometer equipped with a thermoregulated cell holder. Time-resolved Tb^{3+} luminescence spectra were acquired with 100 µs time delay. All measurements were performed with aerated solutions.

Peptide synthesis: Peptides were synthetized on NovaPEG Rink Amide resin (0.46 mmol/g; 0.12 mmol scale) using standard SPPS protocols for Fmoc/tBu chemistry. The first amino acid was attached by single manual coupling, using 3-fold excess of Fmoc-Gly-OH, 2.7-fold excess of HCTU and 6-fold excess of *N*,*N*-diisopropylethylamine (DIEA) in *N*,*N*-dimethylformamide (DMF). This was followed by a capping step (Ac_2O/pyridine/DMF 1:2:7 (v/v/v), 10 mL, 5 min). Removal of the Fmoc protecting group was performed with 20 % piperidine in DMF (3×10 min). Peptide elongation was performed on an automatic peptide synthesizer (CEM Liberty1 Microwave peptide Synthesizer) using double coupling with 4-fold molar excess of Fmoc-L-amino acid, 3.8-fold molar excess of HCTU and 8-fold molar excess of DIEA during 30 min at room temperature. A capping step was performed after each coupling with Ac_2O/DIEA (5 min). Fmoc removal was performed using 20% piperidine in DMF (2×10 min). The phosphoserine was introduced using Fmoc-Ser(PO(OBzl)OH)-OH. Fmoc-L-Glu(OAllyl)-OH and Fmoc-L-Asp(OAllyl)-OH were used to introduce the orthogonally-protected Glu/Asp residue used to graft the chelator on resin for ZFQE and ZFQD respectively. After the final Fmoc removal step, the N-terminus was acetylated by treatment with Ac_2O/pyridine/DMF 1:2:7 (v/v/v, 10 mL, 5 min).

Removal of glutamate or aspartate allyl protecting group: The removal of the allyl protecting group was performed by treating the resin twice with *tetrakis*(triphenylphosphine)palladium(0) ($Pd(PPh_3)_4$) (0.02 mmol, 27.6 mg) and phenylsilane (2.5 mmol, 0.36 mL) in degassed anhydrous DCM (15 mL) for 1 h in the dark.[19] The resin was then washed successively with DCM (4×3 min), DMF (2×3 min), 1% H_2O in DMF (2×3 min), DMF (2×), 1% DIEA in DMF (2×3 min), DMF (2×3 min), sodium diethyldithiocarbamate in DMF (0.12 M, 2×5 min), DMF (2×3 min), DCM (4×3min).

Coupling of the (tBu)-protected macrocyclic ligand: DO3A(*t*Bu)$_3$-propylamine[26] (0.24 mmol, 137.5 mg) was dissolved in DMF (6 mL) and added to the resin (60 µmol) for ZFQE, then a solution of PyBOP (0.24 mmol, 71.15 mg) and DIEA (0.48 mmol, 250.3 µL) in DMF (3 mL) was added. The resin was agitated overnight at room temperature, then washed with DMF (2×), DCM (2×). The same procedure was used for ZFQD (20 µmol) and the reagents were mixed in accordance to the number of equivalents as for the ZFQE presented above (80 µmol of DO3A(*t*Bu)$_3$-propylamine derivative, 80 µmol of PyBOP and 0.16 mmol of DIEA in DMF (1 mL)).

Resin cleavage and removal of protecting groups: Removal of acid-labile protecting groups and resin cleavage were performed using TFA/H_2O/triisopropylsilane/thioanisole (92.5:2.5:2.5:2.5 v/v/v/v, 20 mL) containing dithiotreitol (300 mg) for 4h. TFA was evaporated under reduced pressure and cold diethylether (Et_2O) was added to precipitate the peptide, which was purified by HPLC to give ZFQE (42 mg, 18 % yield) or ZFQD (10 mg, 14 % yield) after freeze-drying. ZFQE: HPLC (anal.) t_R = 6.71 min (method A); LRMS (ESI+) : average *m/z* = 1218.9 (3+), 914.3 (4+), 731.5 (5+), 609.6 (6+), 522.6 (7+) / calculated av. m/z = 1219.68 $[M+3H]^{3+}$, 915.03 $[M+4H]^{4+}$, 732.21 $[M+5H]^{5+}$, 610.34 $[M+6H]^{6+}$, 523.29 $[M+7H]^{7+}$ for M = $C_{157}H_{245}N_{46}O_{49}PS_2$; deconvoluted mass found = 3656.0 / expected mass = 3656.05 (average isotopic composition). ZFQD: HPLC (anal.) t_R = 6.71 min (method A); LRMS (ESI+): average *m/z* = 1214.8 (3+), 911.3 (4+), 729.3 (5+), 607.8 (6+), 521.3 (7+) / calculated av. m/z = 1214.80 $[M+3H]^{3+}$, 911.35 $[M+4H]^{4+}$, 729.28 $[M+5H]^{5+}$, 607.90 $[M+6H]^{6+}$, 521.20 $[M+7H]^{7+}$ for M = $C_{156}H_{243}N_{46}O_{49}PS_2$; deconvoluted mass found = 3641.4 / expected mass = 3642.03 (average isotopic composition).

Metallation with Ln^{3+}: The zinc finger peptide (5.66 µmol, 20.7 mg) and $LnCl_3$ (Ln = Gd or Tb; *ca.* 10 eq.) were dissolved in H_2O and the pH was adjusted to 6.2 using NaOH. The solution was stirred overnight (after 30 min, the pH was controlled and adjusted to 6.2 if needed). Excess of Ln^{3+} was removed using OASIS HLB 3cc (400 mg) LP Extraction Cartridge and the Ln complex was obtained as a white powder after freeze-drying (ca. 65 % yield). LRMS (ESI+): average *m/z* = 1271.08 (3+), 953.83 (4+), 763.33 (5+), 636.33 (6+), 545.42 (7+) / calculated av. m/z = 1271.09 $[M+3H]^{3+}$, 953.57 $[M+4H]^{4+}$, 763.06 $[M+5H]^{5+}$, 636.05 $[M+6H]^{6+}$, 545.33 $[M+7H]^{7+}$ for M = $C_{157}H_{242}N_{46}O_{49}PS_2Gd$; deconvoluted mass found = 3810.24 / expected mass = 3810.28 (average isotopic composition). $ZFQE^{Tb}$: LRMS (ESI+): average *m/z* = 1271.7 (3+), 954.1 (4+), 763.6 (5+), 636.4 (6+), 535.0 (7+) / calculated av. m/z = 1271.65 $[M+3H]^{3+}$, 953.99 $[M+4H]^{4+}$, 763.39 $[M+5H]^{5+}$, 636.33 $[M+6H]^{6+}$, 545.57 $[M+7H]^{7+}$ for M = $C_{157}H_{242}N_{46}O_{49}PS_2Tb$; deconvoluted mass found = 3811.8 / expected mass = 3811.96 (average isotopic composition).

Circular dichroism: Solutions of $ZFQE^{Tb}$ (~ 20 µM) and $ZFQD^{Tb}$ (~30 µM) without Zn^{2+} and with 1.5 eq. Zn^{2+} were prepared in H_2O using a stock solution of the complex. TCEP (250 µM) was added as a reducing agent to ensure cysteine reduction and the pH was adjusted at 7.5 using NaOH. Cuvettes with a 0.4 cm path length were used. Spectra were recorded from 300 nm to 200 nm every 1 nm with a 2 s signal averaging for each point. Each spectrum was recorded twice, averaged and smoothed using a Stavitsky-Golay filter.

Luminescence spectroscopy: Solutions of $ZFQE^{Tb}$ and $ZFQD^{Tb}$ were prepared in a HEPES buffer (10 mM, pH 7.4) containing TCEP (250 µM) as a reducing agent. Typically, the concentration of $ZFQE^{Tb}$ and $ZFQD^{Tb}$ were 20 µM and 100 µM respectively prepared using a stock solution. Zn^{2+} titrations were performed using a $Zn(ClO_4)_2$ solution (2.09 mM in water). For the determination of *q*, the number of water molecules coordinated to Tb^{3+}, solutions of $ZFQE^{Tb}$ (10 µM) and $ZFQD^{Tb}$ (27 µM) in a HEPES buffer (10 mM, pH 7.4) containing TCEP (250 µM) were prepared in various H_2O/D_2O mixtures (25, 50, 75 and 100 % H_2O) without and with 1.5 eq. of Zn^{2+}. Lifetimes in 100 % D_2O were extrapolated from the plot of the rate constants of Tb^{3+} luminescence decay ($k_{Ln} = \tau_{Ln}^{-1}$) against the fraction of H_2O in H_2O/D_2O mixtures (Fig. S3). The number of water molecules coordinated to the Tb^{3+} ion (*q*) was determined using $q = 5 \times (k_{Tb/H2O} - k_{Tb/D2O} - 0.06)$.[27]

Sample preparation for relaxometric studies: All samples were prepared in a HEPES buffer (100 mM, pH 7.4) containing TCEP (25 mM) as a reducing agent. The concentration of $ZFQE^{Gd}$ was determined using the extinction coefficients of tryptophan (ε= 5690 M^{-1} cm^{-1} at 280 nm) and extinction coefficients of tyrosine (ε= 1480 M^{-1} cm^{-1} at 280 nm) and the concentrations of Gd^{3+}-containing solutions were systematically checked by MBS. For Zn^{2+} titration, ^1H relaxivity measurements were performed at 60 MHz and 25°C with [$ZFQE^{Gd}$] = 0.69 mM after addition of a $ZnCl_2$ solution.

NMRD Profiles: All measurements were performed on a Stelar SMARTracer Fast Field Cycling relaxometer (0.01-10 MHz) and a Bruker WP80 NMR electromagnet adapted to variable field measurements (20-80 MHz) and controlled by a SMARTracer PC-NMR console. The temperature was monitored by a VTC91 temperature control unit and maintained by a gas flow. The temperature was determined by previous calibration with a Pt resistance temperature probe. The longitudinal relaxation rates ($1/T_1$) were determined in water. At 400 MHz and 600 MHz, $1/T_1$ measurements were performed in a capillary tube placed in a 5 mm tube containing D_2O using the inversion recovery sequence on a and a Bruker Avance III (400 MHz) equipped with a 5 mm BBO SmartProbe, and a Bruker Avance DMX (200 MHz) equipped with a 5 mm BBIZ probe, respectively. A Bruker Avance 300 MHz and a Bruker Avance III equipped with a 5 mm BBI were used for 300 MHz and 500 MHz respectively. The least-squares fit of the ^1H NMRD data were performed using Visualiseur/Optimiseur[28,29] running on a MATLAB 8.3.0 (R2014a) platform using equations derived below. In the fitting procedure, we have fixed the r_{GdO} distance to 2.50 Å, based on available crystal structure and ENDOR results, the r_{GdH} distance to 3.10 Å and the closest approach of the bulk water protons to the Gd^{3+}, a_{GdH} to 3.5 Å.[30] The quadrupolar coupling constant, $\chi(1+\eta^{2/3})^{1/2}$, has been set to the value for pure water, 7.58 MHz.[31] The diffusion constant has been fixed to 23×10^{-10} m^2 s^{-1} and its activation energy to 10 kJ mol^{-1}. The hydration number was 1 as determined by luminescence lifetime measurements on the Tb^{3+} analogue. The water exchange rate and the water exchange enthalpy were fixed to the values obtained for similar systems ($k_{ex}^{298} = 111\times10^{-6}$ s^{-1} and $\Delta H^{\neq} = 21$ kJ mol^{-1}).[25] The activation energy of the correlation time for the modulation of the zero-field splitting E_V has been fixed to 1 kJ.mol^{-1}. The fitting has been restricted to frequencies above 4.5 MHz as at low magnetic fields the SBM theory fails in describing electronic parameters and rotational dynamics of slowly rotating objects.

Phantom images at 9.4 T: Phantoms of $ZFQE^{Gd}$, Zn-$ZFQE^{Gd}$ and HEPES have been imaged together with a classical Bruker birdcage coil, 35 mm inner diameter, on a BioSpec 9.4 T spectrometer (Bruker, Wissembourg, France). A spin echo sequence was used, to acquire images of each sample with a fixed TE of 9.9 ms and a variable TR ranging from 50 ms to 3000 ms. Using ISA-Tool program, provided with Paravision 5.1, the T_1 relaxation time

of each phantom was calculated, using an exponential fitting, from signal mean intensity measured on the images as function of TR. Background mean intensity, referred to as noise, was also measured. Figure S5 shows the measured mean intensities as function of TR. As noise remains constant, ISA-Tool gives good T_1 estimation. $ZFQE^{Gd}$, $Zn\text{-}ZFQE^{Gd}$ and HEPES have T_1 values of 655 ms, 526 ms, and 2210 ms, respectively.

Acknowledgements

We acknowledge the support from INBS France Life Imaging (grant ANR-11-INBS-0006 from the French ‘‘Investissements d’Avenir’’ program), Agence Nationale pour la Recherche (ANR-22-CE44-0041), DRF impulsion program of the CEA, the Labex Arcane, CBH-EUR-GS (ANR-17-EURE-0003), ITMO Cancer of Aviesan within the framework of 2021-2030 cancer control strategy, on funds administered by INSERM and La Ligue Contre le Cancer (Comités du Loiret, Loire et Cher, Eure et Loire and Morbihan, grants PM-FP/2021-407 and PM-FP/2020-244).

References

1 P. Faller and C. Hureau, *Chem. Eur. J.*, 2012, **18**, 15910–15920.
2 W. N. Lipscomb and N. Sträter, *Chem. Rev.*, 1996, **96**, 2375–2434.
3 K. Nishida and R. Uchida, *J. Immunol. Res.*, 2018, **2018**, e5749120.
4 E. L. Que, R. Bleher, F. E. Duncan, B. Y. Kong, S. C. Gleber, S. Vogt, S. Chen, S. A. Garwin, A. R. Bayer, V. P. Dravid, T. K. Woodruff and T. V. O’Halloran, *Nature Chem*, 2015, **7**, 130–139.
5 S. A. Myers, *Int. J. Endocrinol.*, 2015, **2015**, 1–7.
6 D. Beyersmann and H. Haase, *Biometals*, 2001, **14**, 331–341.
7 S. L. Kelleher, N. H. McCormick, V. Velasquez and V. Lopez, *Adv. Nutr.*, 2011, **2**, 101–111.
8 P. Faller and C. Hureau, *Dalton Trans.*, 2009, 1080–1094.
9 P. Khalighinejad, D. Parrott and A. D. Sherry, *Pharmaceuticals*, 2020, **13**, 268.
10 K. P. Malikidogo, H. Martin and C. S. Bonnet, *Pharmaceuticals*, 2020, **13**, 436.
11 G. Wang and G. Angelovski, *Angew. Chem. Int. Ed.*, 2021, **60**, 5734–5738.
12 M. Isaac, A. Pallier, F. Szeremeta, P.-A. Bayle, L. Barantin, C. S. Bonnet and O. Sénèque, *Chem. Commun.*, 2018, **54**, 7350–7353.
13 E. Pazos, M. Goličnik, J. L. Mascareñas and M. Eugenio Vázquez, *Chem. Commun.*, 2012, **48**, 9534.
14 B. A. Krizek, B. T. Amann, V. J. Kilfoil, D. L. Merkle and J. M. Berg, *J. Am. Chem. Soc.*, 1991, **113**, 4518–4523.
15 A. Klug, *Q. Rev. Biophys.*, 2010, **43**, 1–21.
16 K. Kluska, J. Adamczyk and A. Krężel, *Coord. Chem. Rev.*, 2018, **367**, 18–64.
17 K. Dhingra, P. Fousková, G. Angelovski, M. E. Maier, N. K. Logothetis and É. Tóth, *J. Biol. Inorg. Chem.*, 2008, **13**, 35–46.
18 I. Coin, M. Beyermann and M. Bienert, *Nat Protoc*, 2007, **2**, 3247–3256.
19 N. Thieriet, J. Alsina, E. Giralt, F. Guibé and F. Albericio, *Tetrahedron Lett.*, 1997, **38**, 7275–7278.
20 O. Sénèque and J.-M. Latour, *J. Am. Chem. Soc.*, 2010, **132**, 17760–17774.
21 J. I. Bruce, R. S. Dickins, L. J. Govenlock, T. Gunnlaugsson, S. Lopinski, M. P. Lowe, D. Parker, R. D. Peacock, J. J. B. Perry, S. Aime and M. Botta, *J. Am. Chem. Soc.*, 2000, **122**, 9674–9684.
22 M. V. R. Raju, S. M. Harris and V. C. Pierre, *Chem. Soc. Rev.*, 2020, **49**, 1090–1108.
23 J. L. Major, G. Parigi, C. Luchinat and T. J. Meade, *Proc. Natl. Acad. Sci. U.S.A.*, 2007, **104**, 13881–13886.
24 G. Wang, H. Martin, S. Amézqueta, C. Ràfols, C. S. Bonnet and G. Angelovski, *Inorg. Chem.*, 2022, **61**, 16256–16265.
25 A. Congreve, D. Parker, E. Gianolio and M. Botta, *Dalton Trans.*, 2004, 1441–1445.
26 E. Pazos, M. Goličnik, J. L. Mascareñas and M. Eugenio Vázquez, *Chem. Commun.*, 2012, **48**, 9534.
27 A. Beeby, I. M. Clarkson, R. S. Dickins, S. Faulkner, D. Parker, L. Royle, A. S. de Sousa, J. A. G. Williams and M. Woods, *Journal of the Chemical Society, Perkin Transactions 2*, 1999, 493–504.
28 F. Yerly, *VISUALISEUR 2.3.5*, Switzerland, 1999.
29 F. Yerly, *OPTIMISEUR 2.3.5*, Switzerland, 1999.
30 P. Caravan, J. J. Ellison, T. J. McMurry and R. B. Lauffer, *Chem. Rev.*, 1999, **99**, 2293–2352.
31 B. Halle and H. Wennerstrom, *J. Chem. Phys.*, 1981, **75**, 1928–1943.